Efficient Initialization of Fluxonium Qubits based on Auxiliary Energy Levels

Tenghui Wang,[1,*] Feng Wu,[1] Fei Wang,[1] Xizheng Ma,[1] Gengyan Zhang[1] Jianjun Chen,[1] Hao Deng,[1] Ran Gao,[1] Ruizi Hu[1] Lu Ma,[1] Zhijun Song,[1] Tian Xia,[1] Make Ying,[1] Huijuan Zhan,[1] Hui-Hai Zhao,[2] and Chunqing Deng[1,†]

[1]*DAMO Quantum Laboratory, Alibaba Group, Hangzhou, Zhejiang 311121, China*
[2]*DAMO Quantum Laboratory, Alibaba Group, Beijing 100102, China*

Fast and high-fidelity qubit initialization is crucial for low-frequency qubits such as fluxonium, and in applications of many quantum algorithms and quantum error correction codes. In a circuit quantum electrodynamics system, the initialization is typically achieved by transferring the state between the qubit and a short-lived cavity through microwave driving, also known as the sideband cooling process in atomic system. Constrained by the selection rules from the parity symmetry of the wave functions, the sideband transitions are only enabled by multiphoton processes which require multitone or strong driving. Leveraging the flux tunability of fluxonium, we circumvent this limitation by breaking flux symmetry to enable an interaction between a noncomputational qubit transition and the cavity excitation. With single-tone sideband driving, we realize qubit initialization with a fidelity exceeding 99% within a duration of 300 ns, robust against the variation of control parameters. Furthermore, we show that our initialization scheme has a built-in benefit in simultaneously removing the second-excited state population of the qubit, and can be easily incorporated into a large-scale fluxonium processor.

The initialization of qubits is integral to quantum computing, representing one of the DiVincenzo criteria [1]. Recent studies underscore the considerable impact of both the fidelity and speed of initialization on the effectiveness of quantum error correction (QEC), particularly when frequent reset is required following the measurement of the syndrome qubits [2]. Relying on the natural energy dissipation of the qubit is not only time consuming given increasing qubit coherence times, but also ineffective for low-frequency qubits where thermal excitations can significantly impact the qubit state. As such, active qubit initialization methods have been implemented in various physical platforms for quantum computing [3–6].

In the realm of superconducting quantum circuits, an active initialization can be realized by processing the outcomes of projective measurements [7–10]. However, this method necessitates quantum feedback that requires additional control sources and is ultimately limited by the feedback latency. Alternatively, initialization can be implemented by transferring the qubit state into a dissipative quantum system [11–17], such as a readout cavity. Several protocols have been proposed and demonstrated, which involve bringing the qubit and the cavity into resonance, either adiabatically [11,12] or parametrically [13]. However, these protocols require the qubit to operate at a frequency that is either close to or above the cavity frequency, which limits their application in low-frequency qubits. Alternatively, a sideband transition can be used to transfer the qubit excitation into the dissipative

cavity [15–17]. To comply with the selection rules [18], two weak microwave drivings or a single strong driving is needed to activate the second order transitions when symmetry breaking is absent. More than requiring additional control resources, these microwave drivings could also introduce significant ac-Stark shift [15,16], which complicates the experimental calibration and renders it highly sensitive to the control parameters.

In this work, we present an efficient initialization protocol for fluxonium qubits based on the idea of sideband cooling. As a promising candidate qubit for fault-tolerant quantum computing, fluxonium has garnered significant attention because of its remarkable coherence time [19–21] and its ability to perform high-fidelity two-qubit operations [22–28]. Our protocol takes the advantage of the flux tunability and the rich, anharmonic energy level structure of fluxonium. By displacing the qubit away from its flux degeneracy position [29], we establish a strong coupling between a noncomputational level of the fluxonium and its readout cavity to enable sideband transitions with a weak monochromatic drive. In addition, by adiabatically increasing the driving strength, the auxiliary level acts as a dark state, facilitating the qubit population to be directly transferred into the cavity excitation, thereby significantly enhancing the initialization efficiency. Here, we select the second-excited state as the auxiliary level and achieve ground state initialization with a fidelity exceeding 99% within a duration of 300 ns, robust against the variation of the control parameters. We further show that

230601-1

our scheme can be directly combined with leakage removal on this auxiliary level, and easily extended to initializing multiple qubits through frequency multiplexing.

The fluxonium qubit is capacitively coupled to the readout cavity. The system is described by a coupling Hamiltonian of $H_c = \hbar g_r \hat{n}_q \hat{n}_r / 2$, where $\hat{n}_{r(q)}$ denotes the Cooper-pair number operator of the cavity (qubit). The concept of our protocol is illustrated in Fig. 1(a), where we label the three lowest levels of fluxonium as $|g\rangle, |e\rangle, |f\rangle$ and the n-photon Fock state of the cavity as $|n\rangle$, respectively. The existence of the coupling H_c between the qubit and the cavity hybridizes $|f0\rangle$ and $|g1\rangle$, which are the tensor product states of the composite system. The energy eigenstate (dressed state) $|\overline{g1}\rangle$ contains the fluxonium excitation component $|f0\rangle$, enabling a population transfer from $|e0\rangle$ to $|\overline{g1}\rangle$ via red-sideband driving at the frequency $\omega_r - \omega_{ge}$ and strength Ω_{ef}. Simultaneously, the transferred population in $|\overline{g1}\rangle$ quickly relaxes to the system ground state $|g0\rangle$, due to fast photon dissipation in the cavity. We estimate that the transition rate from $|e0\rangle$ to $|\overline{g1}\rangle$ is proportional to $(\Omega_{ef} g_r / 2\Delta) |\langle g|\hat{n}_q|f\rangle|$ in the dispersive regime, where $\Delta = \omega_{gf} - \omega_r$ [30].

However, at the flux degeneracy position $\varphi_{ext} = \pi$ which is the sweet spot for coherent qubit operations due to its insensitivity to flux noise, the potential has the parity symmetry therefore each eigenstate has well-defined even or odd parity. In particular, $|g\rangle$ and $|f\rangle$ are both even parity wave functions, rendering the rate of the transition $|\langle g|\hat{n}_q|f\rangle|$ to be precisely zero. To enable this direct sideband transition, we temporarily introduce a flux offset $\delta\varphi_{ext}$ to position the qubit at $\varphi_{ext} \neq \pi$ for breaking the parity symmetry. In Fig. 1(b), we illustrate the transition matrix element $\langle g|\hat{n}_q|f\rangle$ (blue line) as well as the sideband-transition frequency $\omega_r - \omega_{ge}$ (orange line), versus $\delta\varphi_{ext}$. As the external flux shifted away from the $\varphi_{ext} = \pi$, the transition matrix element increases significantly until it reaches a maximum value, eventually becoming zero when it reaches another symmetry point at $\varphi_{ext} = 2\pi$. The calculation is based on the qubit parameters extracted from the measured qubit spectrum versus external flux $\omega_{ge}(\varphi_{ext})$ [30].

We first demonstrate microwave activated sideband transitions enabled by symmetry breaking. Starting from the qubit operated at the sweet spot, we prepare the qubit with a $\pi/2$ pulse. A rectangular flux pulse $\delta\varphi_{ext}$ is then applied to shift the qubit slightly away from the sweet spot. Applying a fixed-strength drive for 30 μs, we adjust its frequency detuning and record the ground state population P_{g0} at various values of $\delta\varphi_{ext}$. The drive strength, $\Omega_{ef} \approx 55$ MHz, is inferred from the Rabi rate between states $|e\rangle$ and $|f\rangle$ at the sweet spot. As depicted in Fig. 1(c), the transition occurs when the microwave frequency aligns with the sideband frequency $\omega_r - \omega_{ge}(\delta\varphi_{ext})$. As the qubit shifts away from the sweet spot with increasing $\delta\varphi_{ext}$, the initialization rate, indicated by the width of the measured P_{g0} versus frequency detuning, increases significantly.

We characterize the initialization rate of the qubit population for a wider range of $\delta\varphi_{ext}$ for two specific driving strengths, $\Omega_{ef} \approx 30$ and 55 MHz. As illustrated in Fig. 1(d), the protocol functions effectively for the majority of bias points. Notably, while a stronger drive consistently accelerates the initialization process, an increase in $\delta\varphi_{ext}$ that shifts the qubit away from the symmetry position also enhances the initialization rate. We also detect some nonmonotonic features, indicated by two red arrows in Fig. 1(d). The arrow on the right marks a peak in the initialization rate, signifying an acceleration of initialization due to the coupling with a dissipative two-level system [39,40]. Conversely, at the left point where $\delta\varphi_{ext}/2\pi \approx 0.055$, the sideband frequency $\omega_r - \omega_{ge}$ matches the qubit transition frequency ω_{gf}, leading to a population leakage into the $|f0\rangle$ state and a consequent reduction in initialization efficiency.

While reducing the energy detuning Δ facilitates faster initialization, a small Δ combined with large driving strength Ω_{ef} could induce population leakage to $|f0\rangle$, thereby limit the overall initialization efficiency. To model
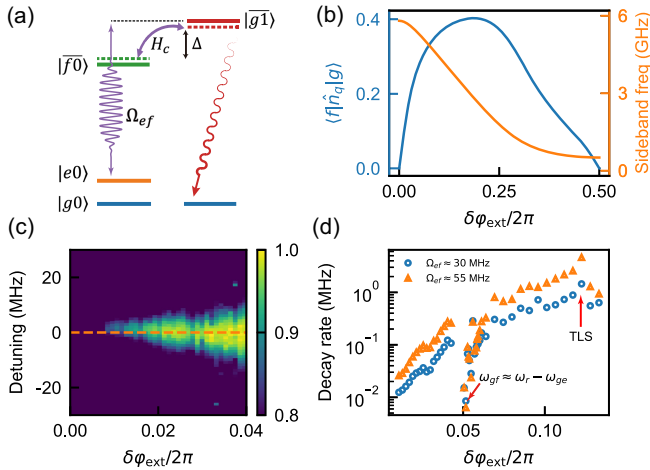

FIG. 1. (a) Energy diagram of the fluxonium-cavity system. The interaction facilitated by $|f0\rangle$ and $|g1\rangle$ allows the transfer of the qubit excitation in $|e0\rangle$ into the dressed state $|\overline{g1}\rangle$ through a sideband drive of strength Ω_{ef} at the frequency detuning Δ. Subsequently, the population returns to the ground state, a result of strong cavity dissipation. (b) Transition matrix element of $\langle f|\hat{n}_q|g\rangle$ and the sideband frequency versus the external flux shift $\delta\varphi_{ext}$ away from the idle position of the qubit at $\varphi_{ext} = \pi$. To initiate the sideband transition, a rectangular flux pulse in conjunction with a constant amplitude microwave drive is applied simultaneously. (c) Ground state population P_{g0} (with readout correction [38]) versus $\delta\varphi_{ext}$ and the detuning respect to the sideband frequency after the application of a 30 μs drive, at $\Omega_{ef} = 55$ MHz. (d) Initialization rate versus $\delta\varphi_{ext}$ under two driving strengths.

the system dynamics, we rewrite the system Hamiltonian in the subspace formed by the energy levels $|e0\rangle$, $|f0\rangle$, and $|g1\rangle$ as

$$H = \frac{1}{2} \begin{bmatrix} 0 & \Omega_{ef} & 0 \\ \Omega_{ef} & 2\Delta & g_{rf} \\ 0 & g_{rf} & -i\Gamma \end{bmatrix}, \quad (1)$$

where $g_{rf} = g_r|\langle g|\hat{n}_g|f\rangle|$ is the effective coupling between $|g1\rangle$ and $|f0\rangle$, and Γ is the photon emission rate of the cavity. Ignoring the non-Hermitian term of $-i\Gamma$, one of the instantaneous eigenstates of the subsystem

$$|\psi_0\rangle = \cos\theta|e0\rangle - \sin\theta|g1\rangle \quad (2)$$

forms a dark state that prevents the leakage of population to the $|f0\rangle$ state, where θ is defined as $\arctan(\Omega_{ef}/g_{rf})$ [41,42]. By adiabatically adjusting θ, the system remains in the $|\psi_0\rangle$ state, thus maximizing state transfer at $\Delta = 0$. This subsequently facilitates the state transfer from $|e0\rangle$ to $|g1\rangle$, without necessitating the excitation of $|f0\rangle$. The non-Hermitian term $-i\Gamma$ contributes an imaginary energy $-(i\Gamma/2)\sin^2\theta$ to $|\psi_0\rangle$, leading to the relaxation of the population in both $|e0\rangle$ and $|g1\rangle$ states out of this subspace and into $|g0\rangle$ [30]. Owing to the minimal nonadiabatic error to the other two eigenstates in the subspace, the total excited population can be approximated as $P_{e0} + P_{g1} \approx \exp[-\Gamma \int_0^T \sin^2\theta(t)dt]$, with T representing the total evolution duration. The time-averaged initialization rate is given by $\Gamma\langle\sin^2\theta\rangle$, which increases as θ increases and is limited by the photon emission rate of the cavity.

The control scheme under discussion is depicted in Fig. 2(a). Throughout the sequence, a flux pulse $\delta\varphi_{ext}$ is utilized to align $|f0\rangle$ and $|g1\rangle$. Flux pulse distortion is corrected employing the method outlined in Ref. [23]. Following a brief delay of $T_{pre} = 10$ ns, we gradually increase θ by increasing the microwave driving strength Ω_{ef} initially, and then sustaining it at a steady level. In order to minimize nonadiabatic transitions, we incorporate a pulse-shaping technique [43] for the envelope [30]. To confirm the feasibility of this adiabatic state transfer, we initially perform a simulation with an initial state of $|e0\rangle$, selecting $\Omega_{ef} = 71$ MHz, $\Delta = 0$, and $T = 500$ ns. As illustrated in Fig. 2(b), the total population $P_{e0} + P_{g1}$ aligns with our analytical model, and the system rapidly transitions to its ground state $|g0\rangle$. Concurrently, the leakage P_{f0} remains minimal and ultimately falls below 10^{-5} at the end of the evolution.

In the conducted experiment, we measure the initialization error of our adiabatic state transfer protocol. The error $e_i = 1 - P_{g0}$ is characterized by comparing the magnitude of the readout signal contrast followed by a Rabi oscillation after state initialization represented as r_{Rabi}, and the maximal value of $|\vec{r}_g - \vec{r}_e|$. Here, $r_{Rabi} = (1 - 2e_i)|\vec{r}_g - \vec{r}_e|$ [30].
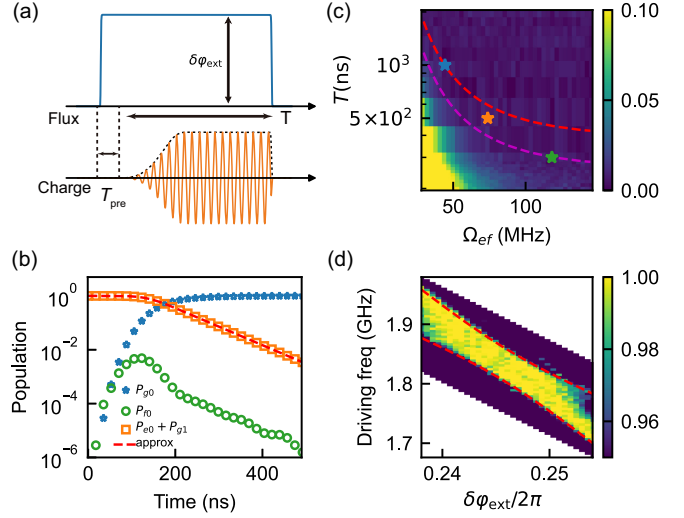

FIG. 2. (a) Control sequence for the initialization with adiabatic state transfer. A rectangular pulse is applied in flux line to bring the qubit into the target $\delta\varphi_{ext}$. The orange line and black dashed line present the microwave waveform and its envelope. The driving strength slowly increase at the initial half duration before stabilizing at a fixed value for the ensuing half. The total driving duration is represented by T, while T_{pre} denotes the advance duration of the flux pulse. (b) Simulation results versus the evolution time. The red dashed line represents the analytic approximation of the population $P_{e0} + P_{g1}$. (c) Initialization error versus the driving strength and duration. Two dashed lines denote the error of 10^{-2} and 10^{-3}, as calculated from the simulation. Three sets of parameters marked with star are selected for statistical characterization. (d) Initialization fidelity versus the driving frequency and the flux offset with $\Omega_{ef} = 71$ MHz and $T = 500$ ns. Two red dashed lines represent the energy level of the two dressed states.

The term $\vec{r}_{g(e)}$ represents the central point of the readout distribution for the ground (excited) state in the IQ plane, which can be inferred by fitting the distribution with a Gaussian [23]. In Fig. 2(c), we present the measured initialization error versus T and Ω_{ef} along with contours corresponding to 10^{-2} and 10^{-3} errors estimated from the simulations. In agreement with the simulations, the measured errors display a decreasing trend as increasing driving strength and duration. According to the simulations, for a large variation of Ω_{ef}, the initialization error can be reduced to below 10^{-2} in less than 1 μs and can be further improved to 10^{-3} in 400–500 ns for $\Omega_{ef} > 100$ MHz. Additionally, we repeat the measurement on three different set of parameters, $\Omega_{ef} = \{43, 71, 114\}$ MHz and $T = \{1000, 500, 300\}$ ns (marked with stars) for statistics purposes. The measured initialization errors are $0.62\% \pm 0.24\%$, $0.66\% \pm 0.19\%$, and $0.63\% \pm 0.21\%$, respectively.

We also employ the measured initialization rate to estimate the lower limits of these errors when the system attains a stationary state, which are 0.072%, 0.042%, and 0.031%, respectively. Detailed information regarding error

statistics and estimations can be found in the Supplemental Material [30]. These lower limits are notably smaller than our measurements. The discrepancy between the experiment and theory might be attributed to the state excitation during readout. Nevertheless, we achieved qubit state initialization with over 99% fidelity within a vast range of Ω_{ef} and T. To further assess the robustness with respect to other parameters, we fix $\Omega_{ef} = 71$ MHz and $T = 500$ ns, and sweep the driving frequency and $\delta\varphi_{\text{ext}}$. The measured fidelity of the initialization are presented in Fig. 2(d). Within the region delineated by the two energy levels of $|\overline{f0}\rangle$ and $|\overline{g1}\rangle$ (indicated by two red dashed lines), we achieve high-fidelity initialization over a frequency span approaching 100 MHz. This initialization scheme requires the presence of a resonance point between $|f0\rangle$ and $|g1\rangle$ in the available flux-tunable range. Such requirement is compatible with the selection of qubit parameters for typical dispersive readout. For some parameter selection where such resonance condition is unavailable, our protocol alternatively allows initialization to the excited state via a blue sideband transition, leveraging the resonance between $|h0\rangle$ and $|e1\rangle$. Moreover, due to the substantial detuning, the driving-induced spurious transitions from $|g0\rangle$ to $|f0\rangle$ are negligible, allowing for a flexible selection of qubit frequencies [30].

Putting this scheme in the context of QEC, we explore its potential in addressing leakage errors and its applicability to the initialization of multiple qubits. Leakage errors, which typically accumulate with the number of gate operations, are generally hard to be detected and subsequently recovered by QEC [12,44,45]. Therefore, it is desirable to eliminate the out of computational-state excitations during qubit initialization [46,47]. The strong resonant interaction between $|f0\rangle$ and $|g1\rangle$ results in the population of $|f0\rangle$ reverting to the ground state via cavity dissipation. We assess the effect of leakage removal by preparing the $|f0\rangle$ state and implementing the initialization protocol with parameters, $T_{\text{pre}} = 10$ ns and $\Omega_{ef} = 114$ MHz. Using the same scheme to characterize initialization errors, the contrast in the detected readout signal can be represented as $r_{\text{Rabi}} = (1 - P_{f0})|\vec{r}_g - \vec{r}_e|$, under the assumption that all initialization errors stem from the leakage population P_{f0}. The efficiency of leakage removal, $1 - P_{f0}$, for a state with maximum leakage (prepared as $P_{f0} = 1$) can be assessed. The observed efficiency for driving duration of $T = 200$ and $T = 300$ ns are 92.7% and 96.4%, respectively. The results reveal that our protocol inherently removes leakage, and its efficiency increases with the driving duration T. An alternative method to improve the efficiency of leakage removal involves extending the resonance duration T_{pre} before the microwave drive [30]. As depicted in Fig. 3, we note damping oscillations in the efficiency relative to T_{pre}, indicative of the population exchange between $|f0\rangle$ and $|g1\rangle$. By extending T_{pre} to
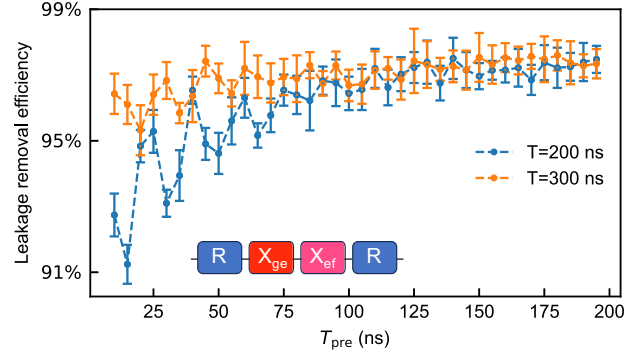

FIG. 3. Leakage removal efficiency versus T_{pre} at $\Omega_{ef} = 114$ MHz. The inset shows the control sequence, where $|f0\rangle$ is prepared by a qubit initialization or reset operation (R) followed by two π pulses, X_{ge} and X_{ef}.

approximately 100 ns, the efficiencies for both $T = 200$ and $T = 300$ ns increase to roughly 98%. The integration of a pre-resonance duration T_{pre} effectively eliminates the population in $|e0\rangle$ and $|f0\rangle$ with high fidelity, offering a straightforward operation for leakage removal in fluxonium qubits.

We ultimately illustrate the simultaneous initialization and operation of multiple qubits using this scheme. To optimize electronic resources, we employ a shared generator for the sideband driving of multiple qubits. For instance, an additional qubit (Q_B) utilizes the same generator as the initial qubit (Q_A) for the initialization, where two sideband driving tones for both qubits are generated via frequency multiplexing and broadcasted to both qubits through a power splitter, connected to both qubits' control lines [30]. To validate the isolation of this initialization scheme among qubits, we employ randomized benchmarking [48,49] to assess the average fidelity of single-qubit gates on one qubit, while concurrently applying repeated initialization operations to another qubit. For Q_A and Q_B, the initialization is achieved using sideband frequencies of
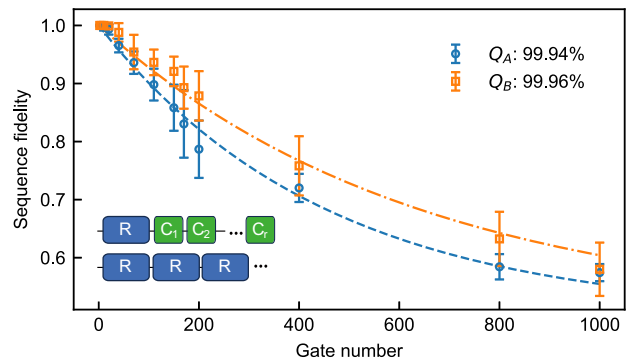

FIG. 4. Single-qubit gate fidelity of Q_A and Q_B characterized by randomized benchmarking, following the simultaneous initialization of both qubits. Each curve is individually obtained while the other qubit undergoes a repeated initialization process.

1.832 and 1.692 GHz, respectively, at $\Delta = 0$. The sideband driving strength and duration are set at 60 MHz and 1 μs for both qubits. The duration of all single-qubit rotations is 20 ns. At the beginning of the sequence, we simultaneously initialize both qubits, attaining fidelities comparable to those observed when the qubits are initialized individually. As presented in Fig. 4, we find no interference with the other qubit's state initialization or single-qubit gate operations while either qubit undergoes repeated initialization. Both Q_A and Q_B display high single-qubit gate fidelity, with the average gate fidelity achieving 99.94% and 99.96%, respectively. These values are consistent with those observed when no initialization operation is performed on the other qubit.

In summary, we demonstrated an efficient initialization scheme for fluxonium qubits, using the sideband cooling technique. By adjusting the external flux of the fluxonium, we disrupt the parity symmetry of the energy eigenstates, which in turn enables an interaction between a noncomputational qubit transition and the cavity excitation. This manipulation facilitates the direct sideband transition with single-tone microwave driving. We further improve the control by adiabatically transferring the qubit excitation to the lossy cavity state, achieving over 99% initialization fidelity within a duration of 300 ns. Finally, we demonstrated our scheme is robust against parameter variations, capable of removing leakages, and applicable to the simultaneous operations of multiple qubits.

Our scheme offers a robust and scalable initialization protocol that can be readily incorporated into a large-scale fluxonium processor, thus constitutes an important technology for the demonstration of quantum error correction with fluxonium qubits.

---

[*] wthzju@gmail.com

[†] dengchunqing@gmail.com

[1] D. P. DiVincenzo, The physical implementation of quantum computation, Fortschr. Phys. **48**, 771 (2000).

[2] Google Quantum AI, Exponential suppression of bit or phase errors with cyclic error correction, Nature (London) **595**, 383 (2021).

[3] C. Monroe, D. M. Meekhof, B. E. King, S. R. Jefferts, W. M. Itano, D. J. Wineland, and P. Gould, Resolved-sideband Raman cooling of a bound atom to the 3d zero-point energy, Phys. Rev. Lett. **75**, 4011 (1995).

[4] V. Vuletić, C. Chin, A. J. Kerman, and S. Chu, Degenerate Raman sideband cooling of trapped cesium atoms at very high atomic densities, Phys. Rev. Lett. **81**, 5768 (1998).

[5] F. Jelezko, T. Gaebel, I. Popa, A. Gruber, and J. Wrachtrup, Observation of coherent oscillations in a single electron spin, Phys. Rev. Lett. **92**, 076401 (2004).

[6] J. M. Elzerman, R. Hanson, L. H. Willems van Beveren, B. Witkamp, L. M. K. Vandersypen, and L. P. Kouwenhoven, Single-shot read-out of an individual electron spin in a quantum dot, Nature (London) **430**, 431 (2004).

[7] J. E. Johnson, C. Macklin, D. H. Slichter, R. Vijay, E. B. Weingarten, J. Clarke, and I. Siddiqi, Heralded state preparation in a superconducting qubit, Phys. Rev. Lett. **109**, 050506 (2012).

[8] D. Ristè, J. G. van Leeuwen, H.-S. Ku, K. W. Lehnert, and L. DiCarlo, Initialization by measurement of a superconducting quantum bit circuit, Phys. Rev. Lett. **109**, 050507 (2012).

[9] Y. Salathé, P. Kurpiers, T. Karg, C. Lang, C. K. Andersen, A. Akin, S. Krinner, C. Eichler, and A. Wallraff, Low-latency digital signal processing for feedback and feedforward in quantum computing and communication, Phys. Rev. Appl. **9**, 034011 (2018).

[10] R. Gebauer, N. Karcher, D. Gusenkova, M. Spiecker, L. Grünhaupt, I. Takmakov, P. Winkel, L. Planat, N. Roch, W. Wernsdorfer et al., State preparation of a fluxonium qubit with feedback from a custom FPGA-based platform, AIP Conf. Proc. **2241**, 020015 (2020).

[11] M. D. Reed, B. R. Johnson, A. A. Houck, L. DiCarlo, J. M. Chow, D. I. Schuster, L. Frunzio, and R. J. Schoelkopf, Fast reset and suppressing spontaneous emission of a superconducting qubit, Appl. Phys. Lett. **96**, 203110 (2010).

[12] M. McEwen, D. Kafri, Z. Chen, J. Atalaya, K. Satzinger, C. Quintana, P. V. Klimov, D. Sank, C. Gidney, A. Fowler et al., Removing leakage-induced correlated errors in superconducting quantum error correction, Nat. Commun. **12**, 1761 (2021).

[13] Y. Zhou, Z. Zhang, Z. Yin, S. Huai, X. Gu, X. Xu, J. Allcock, F. Liu, G. Xi, Q. Yu et al., Rapid and unconditional parametric reset protocol for tunable superconducting qubits, Nat. Commun. **12**, 5924 (2021).

[14] K. Geerlings, Z. Leghtas, I. M. Pop, S. Shankar, L. Frunzio, R. J. Schoelkopf, M. Mirrahimi, and M. H. Devoret, Demonstrating a driven reset protocol for a superconducting qubit, Phys. Rev. Lett. **110**, 120501 (2013).

[15] D. J. Egger, M. Werninghaus, M. Ganzhorn, G. Salis, A. Fuhrer, P. Müller, and S. Filipp, Pulsed reset protocol for fixed-frequency superconducting qubits, Phys. Rev. Appl. **10**, 044030 (2018).

[16] P. Magnard, P. Kurpiers, B. Royer, T. Walter, J.-C. Besse, S. Gasparinetti, M. Pechal, J. Heinsoo, S. Storz, A. Blais, and A. Wallraff, Fast and unconditional all-microwave reset of a superconducting qubit, Phys. Rev. Lett. **121**, 060502 (2018).

[17] H. Zhang, S. Chakram, T. Roy, N. Earnest, Y. Lu, Z. Huang, D. K. Weiss, J. Koch, and D. I. Schuster, Universal fast-flux control of a coherent, low-frequency qubit, Phys. Rev. X **11**, 011010 (2021).

[18] A. Blais, J. Gambetta, A. Wallraff, D. I. Schuster, S. M. Girvin, M. H. Devoret, and R. J. Schoelkopf, Quantum-information processing with circuit quantum electrodynamics, Phys. Rev. A **75**, 032329 (2007).

[19] I. M. Pop, K. Geerlings, G. Catelani, R. J. Schoelkopf, L. I. Glazman, and M. H. Devoret, Coherent suppression of electromagnetic dissipation due to superconducting quasiparticles, Nature (London) **508**, 369 (2014).

[20] L. B. Nguyen, Y.-H. Lin, A. Somoroff, R. Mencia, N. Grabon, and V. E. Manucharyan, High-coherence fluxonium qubit, Phys. Rev. X **9**, 041041 (2019).

[21] A. Somoroff, Q. Ficheux, R. A. Mencia, H. Xiong, R. Kuzmin, and V. E. Manucharyan, Millisecond coherence in a superconducting qubit, Phys. Rev. Lett. **130**, 267001 (2023).

[22] I. N. Moskalenko, I. A. Simakov, N. N. Abramov, A. A. Grigorev, D. O. Moskalev, A. A. Pishchimova, N. S. Smirnov, E. V. Zikiy, I. A. Rodionov, and I. S. Besedin, High fidelity two-qubit gates on fluxoniums using a tunable coupler, npj Quantum Inf. **8**, 130 (2022).

[23] F. Bao, H. Deng, D. Ding, R. Gao, X. Gao, C. Huang, X. Jiang, H.-S. Ku, Z. Li, X. Ma, X. Ni, J. Qin, Z. Song, H. Sun, C. Tang, T. Wang, F. Wu, T. Xia, W. Yu, F. Zhang, G. Zhang, X. Zhang, J. Zhou, X. Zhu, Y. Shi, J. Chen, H.-H. Zhao, and C. Deng, Fluxonium: An alternative qubit platform for high-fidelity operations, Phys. Rev. Lett. **129**, 010502 (2022).

[24] C. Huang, T. Wang, F. Wu, D. Ding, Q. Ye, L. Kong, F. Zhang, X. Ni, Z. Song, Y. Shi, H.-H. Zhao, C. Deng, and J. Chen, Quantum instruction set design for performance, Phys. Rev. Lett. **130**, 070601 (2023).

[25] E. Dogan, D. Rosenstock, L. Le Guevel, H. Xiong, R. A. Mencia, A. Somoroff, K. N. Nesterov, M. G. Vavilov, V. E. Manucharyan, and C. Wang, Two-fluxonium cross-resonance gate, Phys. Rev. Appl. **20**, 024011 (2023).

[26] L. Ding, M. Hays, Y. Sung, B. Kannan, J. An, A. Di Paolo, A. H. Karamlou, T. M. Hazard, K. Azar, D. K. Kim, B. M. Niedzielski, A. Melville, M. E. Schwartz, J. L. Yoder, T. P. Orlando, S. Gustavsson, J. A. Grover, K. Serniak, and W. D. Oliver, High-fidelity, frequency-flexible two-qubit fluxonium gates with a transmon coupler, Phys. Rev. X **13**, 031035 (2023).

[27] X. Ma, G. Zhang, F. Wu, F. Bao, X. Chang, J. Chen, H. Deng, R. Gao, X. Gao, L. Hu, H. Ji, H.-S. Ku, K. Lu, L. Ma, L. Mao, Z. Song, H. Sun, C. Tang, F. Wang, H. Wang, T. Wang, T. Xia, M. Ying, H. Zhan, T. Zhou, M. Zhu, Q. Zhu, Y. Shi, H.-H. Zhao, and C. Deng, Native approach to controlled-Z gates in inductively coupled fluxonium qubits, Phys. Rev. Lett. **132**, 060602 (2024).

[28] H. Zhang, C. Ding, D. K. Weiss, Z. Huang, Y. Ma, C. Guinn, S. Sussman, S. P. Chitta, D. Chen, A. A. Houck, J. Koch, and D. I. Schuster, Tunable inductive coupler for high fidelity gates between fluxonium qubits, PRX Quantum **5**, 020326 (2024).

[29] Y.-x. Liu, J. Q. You, L. F. Wei, C. P. Sun, and F. Nori, Optical selection rules and phase-dependent adiabatic state control in a superconducting quantum circuit, Phys. Rev. Lett. **95**, 087001 (2005).

[30] See Supplemental Material at http://link.aps.org/supplemental/10.1103/PhysRevLett.132.230601, which includes Refs. [31–37] for details of the model, experimental setup, and additional data.

[31] P. Campagne-Ibarcq, E. Flurin, N. Roch, D. Darson, P. Morfin, M. Mirrahimi, M. H. Devoret, F. Mallet, and B. Huard, Persistent control of a superconducting qubit by stroboscopic measurement feedback, Phys. Rev. X **3**, 021008 (2013).

[32] A. D. Córcoles, M. Takita, K. Inoue, S. Lekuch, Z. K. Minev, J. M. Chow, and J. M. Gambetta, Exploiting dynamic quantum circuits in a quantum algorithm with superconducting qubits, Phys. Rev. Lett. **127**, 100501 (2021).

[33] B.-L. Najera-Santos, R. Rousseau, K. Gerashchenko, H. Patange, A. Riva, M. Villiers, T. Briant, P.-F. Cohadon, A. Heidmann, J. Palomo, M. Rosticher, H. le Sueur, A. Sarlette, W. C. Smith, Z. Leghtas, E. Flurin, T. Jacqmin, and S. Deléglise, High-sensitivity ac-charge detection with a MHz-frequency fluxonium qubit, Phys. Rev. X **14**, 011007 (2024).

[34] P. Král, I. Thanopulos, and M. Shapiro, Colloquium: Coherently controlled adiabatic passage, Rev. Mod. Phys. **79**, 53 (2007).

[35] D. I. Schuster, A. Wallraff, A. Blais, L. Frunzio, R.-S. Huang, J. Majer, S. M. Girvin, and R. J. Schoelkopf, ac stark shift and dephasing of a superconducting qubit strongly coupled to a cavity field, Phys. Rev. Lett. **94**, 123602 (2005).

[36] E. Jeffrey, D. Sank, J. Y. Mutus, T. C. White, J. Kelly, R. Barends, Y. Chen, Z. Chen, B. Chiaro, A. Dunsworth, A. Megrant, P. J. J. O'Malley, C. Neill, P. Roushan, A. Vainsencher, J. Wenner, A. N. Cleland, and J. M. Martinis, Fast accurate state measurement with superconducting qubits, Phys. Rev. Lett. **112**, 190504 (2014).

[37] X. Y. Jin, A. Kamal, A. P. Sears, T. Gudmundsen, D. Hover, J. Miloshi, R. Slattery, F. Yan, J. Yoder, T. P. Orlando, S. Gustavsson, and W. D. Oliver, Thermal and residual excited-state population in a 3D transmon qubit, Phys. Rev. Lett. **114**, 240501 (2015).

[38] M. Neeley, R. C. Bialczak, M. Lenander, E. Lucero, M. Mariantoni, A. O'Connell, D. Sank, H. Wang, M. Weides, J. Wenner et al., Generation of three-qubit entangled states using superconducting phase qubits, Nature (London) **467**, 570 (2010).

[39] D. Basilewitsch, R. Schmidt, D. Sugny, S. Maniscalco, and C. P. Koch, Beating the limits with initial correlations, New J. Phys. **19**, 113042 (2017).

[40] H. Sun, F. Wu, H.-S. Ku, X. Ma, J. Qin, Z. Song, T. Wang, G. Zhang, J. Zhou, Y. Shi, H.-H. Zhao, and C. Deng, Characterization of loss mechanisms in a fluxonium qubit, Phys. Rev. Appl. **20**, 034016 (2023).

[41] L. Giannelli and E. Arimondo, Three-level superadiabatic quantum driving, Phys. Rev. A **89**, 033419 (2014).

[42] B. T. Torosov, G. Della Valle, and S. Longhi, Non-Hermitian shortcut to stimulated Raman adiabatic passage, Phys. Rev. A **89**, 063412 (2014).

[43] J. M. Martinis and M. R. Geller, Fast adiabatic qubit gates using only σ_z control, Phys. Rev. A **90**, 022307 (2014).

[44] J. Ghosh, A. G. Fowler, J. M. Martinis, and M. R. Geller, Understanding the effects of leakage in superconducting quantum-error-detection circuits, Phys. Rev. A **88**, 062329 (2013).

[45] M. Suchara, A. W. Cross, and J. M. Gambetta, Leakage suppression in the toric code, in *2015 IEEE International Symposium on Information Theory (ISIT)* (IEEE, New York, 2015), pp. 1119–1123, 10.1109/ISIT.2015.7282629.

[46] F. Battistel, B. M. Varbanov, and B. M. Terhal, Hardware-efficient leakage-reduction scheme for quantum error correction with superconducting transmon qubits, PRX Quantum **2**, 030314 (2021).

[47] J. F. Marques, H. Ali, B. M. Varbanov, M. Finkel, H. M. Veen, S. L. M. van der Meer, S. Valles-Sanclemente, N. Muthusubramanian, M. Beekman, N. Haider, B. M. Terhal, and L. DiCarlo, All-microwave leakage reduction

units for quantum error correction with super-conducting transmon qubits, Phys. Rev. Lett. **130**, 250602 (2023).

[48] E. Knill, D. Leibfried, R. Reichle, J. Britton, R. B. Blakestad, J. D. Jost, C. Langer, R. Ozeri, S. Seidelin, and D. J. Wineland, Randomized benchmarking of quantum gates, Phys. Rev. A **77**, 012307 (2008).

[49] E. Magesan, J. M. Gambetta, and J. Emerson, Characterizing quantum gates via randomized benchmarking, Phys. Rev. A **85**, 042311 (2012).